ACS APPLIED MATERIALS & INTERFACES

www.acsami.org

Research Article

Core–Shell Nanohydrogels with Programmable Swelling for Conformance Control in Porous Media

Liyuan Zhang, Alireza Abbaspourrad, Shima Parsa, Jizhou Tang, Flavia Cassiola, Meng Zhang, Shouceng Tian, Caili Dai, Lizhi Xiao,* and David A. Weitz*

Cite This: *ACS Appl. Mater. Interfaces* 2020, 12, 34217–34225

Read Online

ACCESS | Metrics & More | Article Recommendations | Supporting Information

ABSTRACT: Conformance control during waterflooding in an oil reservoir is utilized to redistribute water and increase the sweep efficiency and hence oil production. Using preformed gel particles can effectively redirect the flow by blocking the high-permeability zones and forcing water into low-permeability zones where the oil is trapped. However, the size of such gel particles can limit their applications deeper within the reservoir and can result in shear-induced degradation near the well bore. Here, we fabricate core–shell nanohydrogels with delayed swelling behavior; their volume increases by a factor of 200 after about 30 days in brine under reservoir conditions. We study their effect on the flow behavior in a three-dimensional porous medium micromodel consisting of randomly packed glass beads. Using confocal microscopy, we directly visualize the spatial variations of flow in the micromodel before and after nanohydrogel injection and swelling. The swollen nanohydrogels block some pores reducing the permeability of the micromodel and diverting the water into low-permeability regions. A core flood experiment further confirms that the nanohydrogels can significantly reduce the permeability of a reservoir sample and divert the fluid flow. Our results demonstrate that these core–shell nanohydrogels might be useful for flow control in porous media and can be used as a conformance control agent.

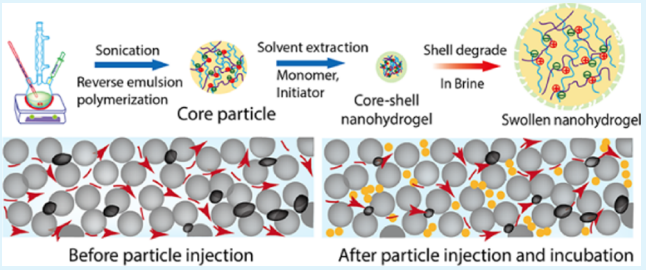

KEYWORDS: *core–shell nanohydrogels, delayed swelling, conformance control, porous media, core flood test*

1. INTRODUCTION

Recovery of crude oil is always limited, even in the best of reservoirs, with amounts as large as 70% of the original crude left in place, even after the use of the most standard recovery method, the injection of water to displace the crude oil in the reservoir.[1,2] The origin of this low displacement ratio lies in the mismatch in the viscosities of the displacing fluid with that of the crude and in the intrinsic heterogeneity of the reservoir. The mismatch in viscosity results in an inherent flow instability, viscous fingering, where the displacing fluid flow forms channels through which it is transported in the reservoir, leaving large quantities of oil behind.[3,4] This is exacerbated by heterogeneities in the porous medium, where the fluids flow through regions of high permeability, bypassing all of the oil in the neighboring regions of low permeability.[5,6] The combination of these effects leads to very poor sweep efficiency, resulting in large amounts of residual oil left in place. This motivates the use of many different techniques for enhanced oil recovery.[7−23] One important feature of these methods is to improve the sweep efficiency by improving conformance by reducing flow in the regions of high permeability to force the displacing fluid into regions of lower permeability, where much of the residual oil lies. Many techniques for conformance control have been developed.[17−26] One of the most promising approaches is the use of preformed particles such as submicron- to micron-sized polymeric gel particles, insoluble but completely dispersible in water and stable for up to one year at reservoir conditions, including the higher temperatures found in each reservoir.[20−26] While dispersed in water, these particles can be injected and penetrate into the porous medium, blocking pore throats and increasing the resistance of the high-permeability paths, thereby diverting the fluid to zones with low permeability, which are more poorly swept. This process requires sufficient particles with sizes larger than the pores to be transported into the reservoir to block the high-permeability paths. However, it is difficult to deliver sufficient particles deep into the zone where most residual oil is located due to the relatively large particle size, which causes them to be trapped in pore throats near the injection well rather than deeper within the reservoir where they are most needed. One way to force these particles to be transported deep into the reservoir is to increase the injection pressure, which deforms the particles enabling them to pass through the pore

Received: June 1, 2020
Accepted: July 7, 2020
Published: July 7, 2020

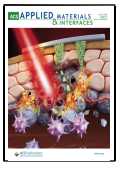

https://dx.doi.org/10.1021/acsami.0c09958
ACS Appl. Mater. Interfaces 2020, 12, 34217–34225

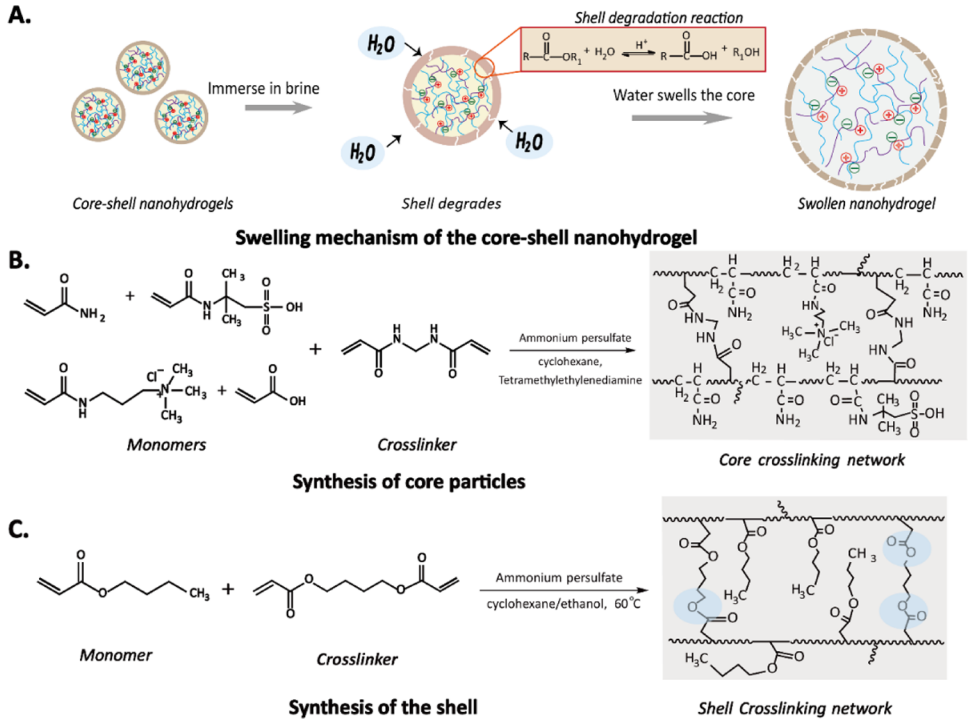

Figure 1. Synthesis of core−shell nanohydrogels. (A) Swelling mechanism of the core−shell nanohydrogel. The inner yellow region represents the core particle and the brown circle represents the shell. After the nanohydrogels are suspended in brine at 50 °C, the shell starts to degrade, and the water penetrates inside the core to gradually swell the nanohydrogel. (B) Synthesis reaction of the hydrogel core particle. (C) Synthesis reaction of the shell on the core particle.

throats.[4,10] There is a threshold pressure for sufficient deformation to occur, which depends on the ratio of the particle size to pore throat size, as well as the mechanical properties of the particles.[23,27,28] However, relying on this threshold pressure to deliver particles into the deep zone of the reservoir is technically challenging because of the limitations to the injection pressure. Moreover, deformation of the particles while they are transported due to the high pressure can make them lose their ability to block high-permeability regions.[4,28] This is particularly problematic near the well bore, where the shear forces are the highest and can degrade the hydrogel particles.[28] Thus, there remains a need to fabricate particles that can be easily transported and penetrate deep into the reservoir but then block pores and effectively divert fluid into low-permeability regions. This would also allow more economic use of particles, as they would be trapped only in the regions of the reservoir where they are most required.

Here, we introduce a new strategy to address the needs of microparticles for conformance control for oil recovery. We fabricate core−shell nanohydrogels that exhibit a delayed swelling: they are initially very small and can easily penetrate through the pores, allowing them to be transported deep into the reservoir. After a controlled time, they swell and become large enough to block the pores. These nanohydrogels have a hydrophilic crosslinked core and a degradable shell. While initially dispersed in aqueous solution, these nanohydrogels maintain their original size and integrity for many days, with the time depending on the shell thickness, allowing them to travel deep into the reservoir. Upon shell degradation, the hydrogel core uptakes water and swells to its ultimate capacity, which makes it large enough to effectively block the pores. We demonstrate the utility of these nanohydrogels by injecting them into a three-dimensional (3D) micromodel porous medium consisting of packed glass beads and observing flow patterns using confocal microscopy. The appearance of new flow streams in the previously poorly swept regions confirms the effectiveness of the nanohydrogels in blocking high-permeability zones and redirecting the flow of the displacing fluid into low-permeability zones. We also conduct a core flood test using these nanohydrogels and show that the permeability of the core is significantly decreased after injection and swelling of the nanohydrogels. These results establish a proof of concept that this approach can be developed successfully.

2. RESULT AND DISCUSSION

2.1. Synthesis of Core−Shell Nanohydrogels. We fabricate nanohydrogels with a core−shell structure that exhibit delayed swelling under typical reservoir conditions for conformance control. The main composition of the core of the nanohydrogels is polyacrylamide, while the shell is made of butyl acrylate crosslinked by 1,4-butanediol diacrylate. Upon suspending the nanohydrogels in brine at 50 °C, the ester bonds in the shell hydrolyze over time, causing the shell to degrade and enabling water to permeate the core, causing it to swell (Figure 1A).[29] To produce this structure, we use a two-step process, initially fabricating the core and subsequently coating it with the shell material. We generate water-in-oil emulsions as the templates for fabricating the core particles using an ultrasonic processor for 2 min. The water phase contains four types of monomers: acrylamide, acrylic acid, 2-acrylamido-2-methyl-1-propanesulfonic acid sodium salt, and (3-acrylamidopropyl)trimethylammonium chloride. We also dissolve *N*,*N*′-methylene bisacrylamide and ammonium persulfate (APS) in the water to serve as the crosslinker and initiator, respectively. The oil phase is cyclohexane with Span 80 as the surfactant for the emulsion. To enhance the swelling

https://dx.doi.org/10.1021/acsami.0c09958
ACS Appl. Mater. Interfaces 2020, 12, 34217−34225

of the nanohydrogels, we combine strong positive and negative charged monomers as core components. These charged monomers enhance the hydrophilic character of the core increasing the degree of swelling while also enhancing the thermal stability. Before swelling, they form a crosslinked ionic structure in the core; this delays the swelling even after water penetrates, increasing the penetration of the nanohydrogels into the reservoir.[30−36] To maximize the swelling, we use as high an initial monomer concentration as possible, 50 wt %.[31,34] After emulsification, we maintain the emulsion at 65 °C in an oil bath with vigorous stirring to polymerize the monomers with the crosslinker to form the core particles. To control the crosslinking density and consequently the swellability of the nanohydrogels, we vary the molar ratio of the monomers and crosslinker. Since these crosslinked particles are formed in a fully hydrated state, it is necessary to dehydrate them to reduce their size prior to coating them with the shell. This is achieved by adding a mixture of ethanol/cyclohexane with a 1:1 volume ratio to the oil phase. The addition of ethanol extracts water from the core by increasing the water solubility in the oil phase; this results in shrinkage of the particles. We then add butyl acrylate and 1,4-butanediol diacrylate with a molar ratio of 10:1 into the external oil phase. The amphiphilic butyl acrylate has an affinity to the hydrogel−oil interface, which concentrates on the surface of the dehydrated core particles. As the initiator, we use ammonium persulfate; it is water-soluble and hence is concentrated in the hydrogel core of the particles, thereby further limiting polymerization of the shell to the surface of the particles, rather than in the bulk oil phase. We form the shell by stirring the emulsion overnight and maintaining it at 70 °C. After the shell is formed, we cool the reaction mixture, centrifuge the nanohydrogel suspension to remove the oil phase, wash the particles with ethanol several times, and dry them in a desiccator for 2 days at room temperature. The chemical structure of monomers and crosslinkers as well as the reactions that form the crosslinked network of the hydrogel core and shell are shown in Figure 1B,C.

2.2. Tuning Synthetic Parameters for Controlling the Core and Shell. Our goal in formulating these nanohydrogels is to create particles that are initially small enough that they can be easily transported deep into the reservoir where they encounter the residual oil. Once they have been transported within the reservoir, the nanohydrogels swell to become large enough to block the pores and modify the conformance of the reservoir. Thus, the initial size of the nanohydrogels should be as small as possible to enable them to freely pass through the pores. To control the initial size of the nanohydrogels, we vary the surfactant concentration, which controls the size of the emulsion drops when the particles are formed. In addition, the size of the nanohydrogels after they swell should be as large as possible to optimize the conformance control. To vary the swollen size of the nanohydrogels, we control the degree of swelling by varying the ratio of monomer to crosslinker. In addition, to control the time scale upon which the swelling occurs, we vary the shell thickness through varying the shell monomer. We fix the monomer to crosslinker ratio at 160:1 and synthesize nanohydrogels using a 3 wt % surfactant with shell material concentration at 0.5 mol L^{-1}. To visualize the size and the morphology of nanohydrogels produced, we use scanning electron microscopy (SEM). They have a spherical shape with diameters of ∼150 nm, as shown in Figure 2A. To verify the core−shell structure of these nanohydrogels, we use

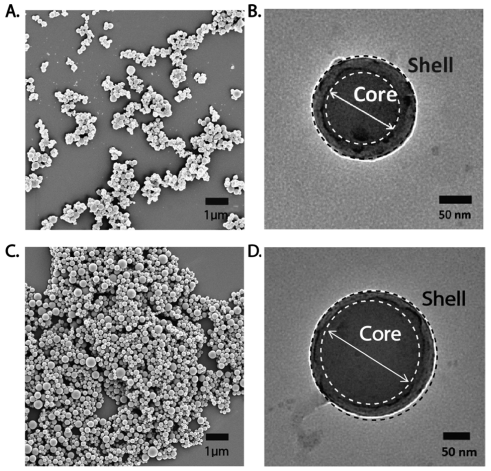

Figure 2. Characterization of core−shell nanohydrogel by SEM and TEM. (A, B) SEM and TEM images of nanohydrogels with different sizes ∼150 nm. (C, D) SEM and TEM images of nanohydrogels with a size of ∼250 nm.

transmission electron microscopy (TEM) to determine their core size and shell thickness. We observe a clear boundary that delineates the core and shell. Nanohydrogels with a size of ∼150 nm in Figure 2A have a core that is roughly 100 nm with a shell that is roughly 25 nm, as shown in Figure 2B. To vary the nanohydrogel size, we decrease the surfactant concentration to 1 wt % and the shell material concentration to 0.15 mol L^{-1} and again use SEM and TEM to examine the morphology and shell thickness. Now, the nanohydrogels have a core of ∼220 nm and a shell of ∼15 nm for a total size of ∼250 nm, as shown in Figure 2C,D. These results indicate that increasing surfactant concentration while generating core emulsion templates results in smaller core particles; increasing shell monomer concentration produces a thicker shell. Overall, we can control the nanohydrogel size as well as its shell thickness by tuning different reaction parameters, such as the emulsification time and the polymerization time while generating the emulsion for core particles and the polymerization time for growing shell.

2.3. Swelling Behavior and Rheological Property of Core−Shell Nanohydrogels. Several parameters determine the swelling profile of the nanohydrogel under reservoir conditions; these include the molar ratio between core monomers and crosslinkers and the thickness of the shell. To measure the swelling, we disperse the nanohydrogels with a size of ∼250 nm in brine at 50 °C for 30 days and measure their sizes by dynamic light scattering (DLS) at different points during this time interval. The sizes of these nanohydrogels do not change significantly in the first few days but then gradually increase starting on day 5. After 30 days, they are swollen by a factor of more than 6 in radius, to a value of 1.6 μm, as indicated by the red dots in Figure 3A. The delay in the swelling is due to the hydrophobic shell that minimizes water diffusion into the core, preventing swelling initially, while allowing water to penetrate and swell the hydrogel core once the shell has degraded. To vary the amount of swelling, we change the ratio of the monomer to crosslinker of the core particle in the nanohydrogels. When we use a ratio 75:1, the size of the fully swollen nanohydrogels is reduced to about 1.0 μm, as shown by the black squares in Figure 3A. By comparison, when we increase the ratio to 300:1, the size of

https://dx.doi.org/10.1021/acsami.0c09958
ACS Appl. Mater. Interfaces 2020, 12, 34217−34225

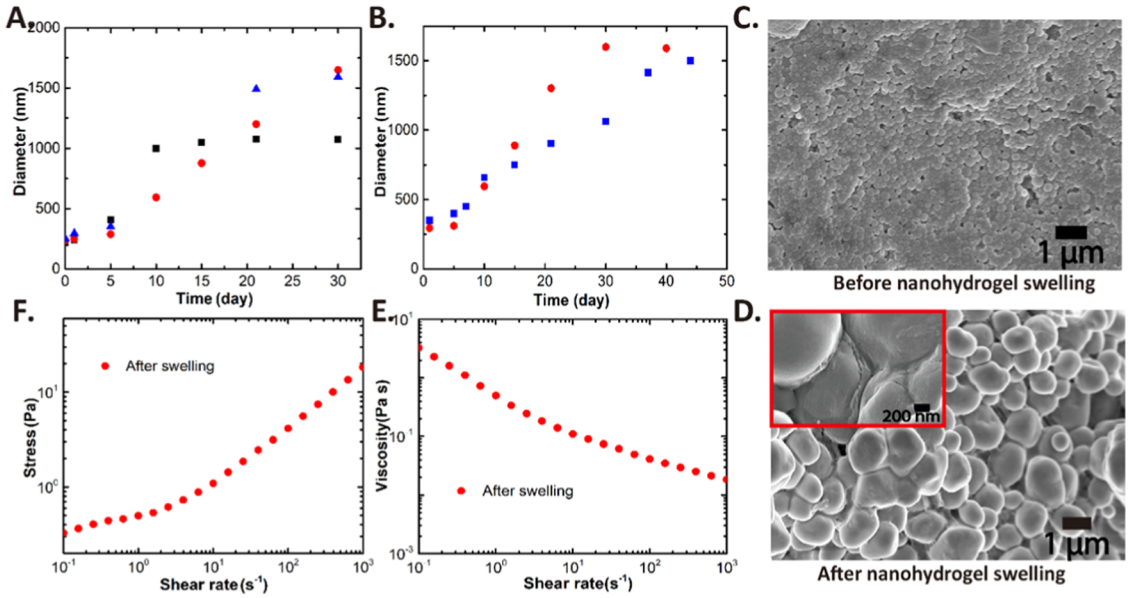

Figure 3. Swelling behavior and rheological property of core−shell nanohydrogels. (A) DLS measurement of the nanohydrogel size at different time intervals for 75:1 (solid black squares), 160:1 (solid blue triangles), and 300:1 (solid red circles) nanohydrogels possessing a 15 nm thick shell. (B) DLS measurement of 160:1 nanohydrogels with different shell thicknesses of ∼15 nm (solid red circles) and ∼30 nm (solid blue squares). (C, D) SEM images of the nanohydrogels with a diameter of 250 nm and a 15 nm shell before swelling and after swelling in brine at 50 °C, respectively. (E) Stress as a function of shear rate of 1 wt % nanohydrogel with a diameter of 250 nm when just dispersed in brine. (F) Stress as a function of shear rate of 1 wt % swollen nanohydrogel suspension.

the swollen nanoparticles is almost the same as 160:1 nanohydrogels, as shown by the blue triangles in Figure 3A; we believe that this is a result of the high salinity of the fluid, which limits the total swelling.

To investigate the effect of the shell thickness on the swelling profile, we fix the ratio of core monomers to crosslinker at 160:1 and increase the concentration of the shell materials to 0.6 mol L^{-1}. This results in nanohydrogels with a diameter of ∼350 nm and a shell of ∼30 nm (Supporting Information, Figure S1). When dispersed in brine at 50 °C, these nanohydrogels exhibit a delayed increase in size, starting only at day 7, and then gradually swelling over 40 days, as shown by the blue squares in Figure 3B. Thus, the increased shell thickness further delays the diffusion of water into the hydrophobic shell, slowing the initial swelling of the particles. When the core particles contact water after the shell degrades, the charged monomers in the core do not hydrolyze, thus slowing down the degradation of the nanohydrogel polymer. Moreover, the presence of sulfonated monomers and amine monomers form an ionic crosslinking structure, which further delays the swelling and enhances the thermal stability of the nanohydrogels.[28] To further study the morphology of these nanoparticles, we freeze-dry the nanohydrogels to maintain their structures before and after swelling and directly visualize them using SEM. These nanohydrogels when just dispersed in brine (Figure 3C) are significantly smaller than those of the fully swollen state (Figure 3D). Moreover, we observe the evidence of shell breakage in the inset image in Figure 3D, confirming the degradation of the shell.

2.4. Nanohydrogel for Fluid Diversion in 3D Micromodel Porous Medium. To investigate the properties of these nanohydrogels in fluid diversion, we prepare a sample of the 160:1 nanohydrogels with a size of ∼250 nm at 1 wt % in brine. This is the same total polymer concentration of polymer that is typically used for conformance control in reservoir applications. Since the polymer is initially in a highly compressed state within the nanoparticles, the initial volume fraction of nanohydrogels is low, about 1%, and, as a result, the viscosity of the suspension is essentially the same as that of the brine without particles, about 10^{-3} Pa s (Supporting Information, Figure S2). The low viscosity and small particle size facilitate the transport of the nanohydrogels to a greater depth in a reservoir.[14,15,37] The total polymer concentration is sufficiently high to influence conformance upon swelling of the nanohydrogels. To determine the effects of swelling, we hold the suspension at 50 °C for 30 days, whereupon the volume of the nanohydrogels increases by more than 200 times compared with their volume when initially dispersed in brine. The effective volume fraction is then greater than 1, which implies that the nanohydrogels must deform to pack in the suspension. This results in dramatic changes in the rheological properties of the suspension. For example, the viscosity at very low shear rates appears to diverge and has a value of 3 Pa s at a shear rate of 0.1 s^{-1}, the lowest value measured; this is more than 1000 times larger than the viscosity of the suspension before swelling and reflects the much larger size of the hydrogels and the very high packing that results. The suspension also exhibits pronounced shear thinning as the shear rate increases to about 10 s^{-1}, as shown in Figure 3E.[38] Further insight is obtained by plotting the shear stress as a function of shear rate. The stress decreases linearly with shear rate until ∼10 s^{-1}, whereupon the stress becomes nearly independent of shear rate. This behavior is consistent with that of a yield stress fluid with a yield stress of about 0.3 Pa, as shown in Figure 3F, again reflecting the compression of the hydrogels upon swelling. This is also the behavior required for the use of this form of polymer for conformance control.

To directly investigate the role of these nanohydrogels in conformance control, we use a 3D micromodel porous medium made by sintering randomly packed glass beads with

https://dx.doi.org/10.1021/acsami.0c09958
ACS Appl. Mater. Interfaces 2020, 12, 34217−34225

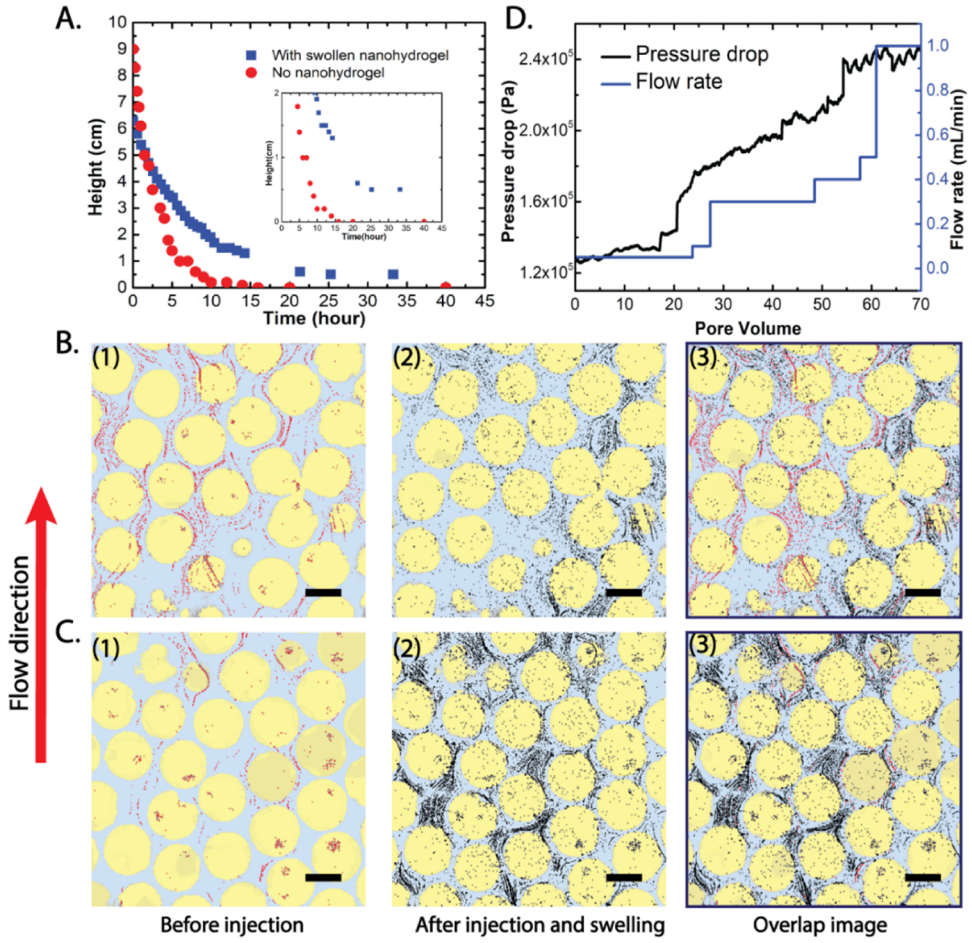

Figure 4. Nanohydrogel for conformance control before and after nanohydrogel injection and swelling in 3D micromodel at the pore scale. (A) Height under which the fluid passes through the micromodel as a function of time. The inset image is the zoom-in image while the height is less than 2 cm. (B, C) Images of two locations chosen at random, 2 mm along the x direction apart. (B(1), C(1)) Flow patterns before 250 nm nanohydrogel injection. Red lines are the tracer particle pattern representing the flow pattern. (B(2), C(2)) Flow patterns represented by the black lines after 250 nm nanohydrogel injection and fully swelling after one month. (B(3), C(3)) Overlap images of (B(1)) with (B(2)) and (C(1)) with (C(2)). Yellow disks represent glass beads. The scale bar is 100 μm. (D) Pressure drop of the Bentheimer core as a function of flow rate during brine injection after 47 days.

a radius of 32 μm in a square quartz capillary tube. The length of the micromodel is L = 3 cm, while its cross-sectional area is A = 9 mm^2 and its porosity is $\varphi \sim 41\%$.[39,40] We measure the flow through the micromodel by setting the hydrostatic pressure at the inlet and using a balance to measure the time taken for a fixed mass of fluid, ∼50 mg, to exit the micromodel. This corresponds to roughly half a pore volume of fluid. We set the hydrostatic pressure at the inlet by adjusting the height of the fluid reservoir. We measure the flow of pure brine through the micromodel and find the height to depend approximately on the inverse of the transit time, as shown by the circles in Figure 4A. This is expected from Darcy's law, where the permeability is

$$\kappa = \frac{\mu Q L}{A\ \Delta P} \tag{1}$$

where μ is the viscosity of the brine, $\sim 10^{-3}$ Pa s, Q the flow rate, and ΔP is the pressure drop. From these data, we estimate that the permeability of the micromodel is 4×10^{-14} m^2. To measure the effects of the nanohydrogels, we use the 160:1 nanohydrogels with an unswollen radius of 250 nm and suspend them in the brine at a concentration of 1 wt %. We flow several pore volumes of this suspension through the micromodel, stop the flow, and seal the sample. We then maintain the sample at 50 °C for 30 days to allow the nanohydrogels to fully swell. When we repeat the flow measurements, we find a noticeable decrease in the permeability as the flow is slower, as shown by the squares in Figure 4A. Moreover, at the lowest pressure, the flow seems to saturate and the time scale gets longer with the data of the pressure never falling to zero, as highlighted in the inset in Figure 4A. Interestingly, the height where the data saturate is about 0.5 cm, which corresponds to a pressure of 50 Pa. Given that this is the pressure drop across the whole micromodel, this would correspond to a pressure drop of about 0.5 Pa, which is the yield stress of the swollen nanohydrogel sample, across a length of about 300 μm. This behavior is consistent with there being yield stress within the micromodel due to the nanohydrogels blocking the pores. These low-pressure measurements were done after the high-pressure measurements, which presumably displaced some of the microgels. Indeed, if we begin with the low-pressure measurements, to test the micromodel completely filled with the swollen particles, we find that we must do so to even higher pressures to initiate a noticeable flow rate, again consistent with the yield

https://dx.doi.org/10.1021/acsami.0c09958
ACS Appl. Mater. Interfaces 2020, 12, 34217−34225

stress behavior of the rheology observed for the swollen particles.

To gain further insight into the behavior of the swollen nanohydrogels, we also directly visualize the fluid flow through the micromodel using a confocal microscope. For this, we use a micromodel with larger pore sizes fabricated using glass beads of 75 μm radius but the same length, cross-sectional area, and porosity as the previous one. We measure the permeability to be $\kappa \sim 8.5 \times 10^{-10}$ m^2. We formulate a fluid, which is a mixture of 88 wt % dimethyl sulfoxide (DMSO) and 12 wt % water, to which we add 0.005 wt % 1 μm fluorescent tracer particles. This fluid matches the refractive index of glass beads, enabling full visualization of flow through the pores.[40] We use confocal microscopy to visualize the flow patterns at the pore scale. This visualization is easier because we use the larger bead size. We flow the index-matching fluid into the 3D micromodel using a syringe pump at a flow rate of 100 μL h^{-1}. To construct the flow pattern, we record a video of the fluid using confocal microscopy for 3 min in the *xy* plane, at 15 frames s^{-1}, and at a fixed focal plane (*z* position). We use ImageJ to stack all frames into a single image, in which the tracer particle pattern represents the fluid pattern. To visualize the flow at different positions in the micromodel, we acquire additional videos at the same *z* position but at different locations in the *xy* plane. The flow patterns, denoted by the red lines, at two locations are shown in Figure 4B(1),C(1). We observe that tracer particles appear in pores where most flow passes through, while some pores have few tracer particles, indicating less fluid invading these areas. To investigate the modifications in the flow pattern induced by the swollen nanohydrogels, we use a suspension of the 160:1 nanohydrogels with a diameter of 250 nm and prepare a suspension at 1 wt % in brine. We flush the micromodel with brine to remove the index-matched probe fluid and inject 1 pore volume of the nanohydrogel suspension into the micromodel, seal it, and maintain it at 50 °C for 30 days to fully swell the nanohydrogels. The permeability after the nanohydrogels have been swollen is measured using brine as a displacing fluid and is 6×10^{-10} m^2. This result indicates that 1 pore volume of the nanohydrogel suspension after swelling in the micromodel can significantly reduce its permeability, by ∼30%, presumably because some pores become blocked and the fluid must find different flow paths through the porous medium. To confirm this hypothesis, we inject the tracer particle-laden, index-matched fluid at a flow rate of 100 μL h^{-1} into the micromodel and obtain tracer particle patterns at the same locations as we did before nanohydrogel injection; these are represented by black lines, as shown in the confocal images of Figure 4B(2),C(2). The significant difference in the fluid flow pattern before and after the nanohydrogel swelling is directly observed by the overlapped images, as shown in Figure 4B(3),C(3). Comparing the position of red and black lines, it is clear that more tracer particles appear in previously poorly swept areas after nanohydrogel swelling, demonstrating the efficacy of the swollen nanohydrogels at diverting the fluid. These results clearly show the efficacy of these nanohydrogels in conformance control.

2.5. Coreflooding Using Nanohydrogel for Conformance Control. To evaluate the efficacy of the nanohydrogels for reservoir applications, we use a rock sample and perform a core flood test. We inject 8 pore volumes of suspension of 1 wt % 250 nm diameter nanohydrogel particles in brine into a Bentheimer sandstone core sample, with a permeability of 1.2 $\times 10^{-12}$ m^2, at a flow rate of 6×10^4 μL h^{-1}, and at a temperature of 50 °C chosen to match the temperature of several reservoirs. After a little over 1 pore volume of injected fluid, the concentration of nanohydrogels in the recovered fluid rises to the same value as that injected, confirming that the nanohydrogels pass freely through the pores with no loss (Supporting Information, Figure S3). We then stop the flow, seal the core, and maintain the temperature at the reservoir temperature of 50 °C for over 1 month to fully swell the particles. We then flood the core with pure brine and measure the pressure drop as the flow rate is varied, as shown in Figure 4D. The rock permeability, calculated by Darcy's law, decreases significantly. At a flow rate of 3×10^3 μL h^{-1}, the rock permeability is 8.2×10^{-16} m^2. Moreover, the permeability varies with time, increasing to 3.5×10^{-15} m^2 when the flow rate is 1.8×10^4 μL h^{-1} and 9.0×10^{-15} m^2 when the flow rate is 6×10^4 μL h^{-1}; thus, the permeability is dependent on flow rate. We hypothesize that this behavior is caused by the displacement of the nanohydrogels within the core. Increasing the injection flow rate of brine causes the deformation of nanohydrogels propagating through the pores, resulting in increased permeability. We also observe pronounced fluctuations in the pressure drop when the flow rate is higher than 2.4×10^4 μL h^{-1}, as shown in Figure 4D. This could be caused by the nanohydrogels temporarily blocking the pores, which induces high pressure drops, but then quickly releasing as the nanohydrogels deform and pass through pores. During this process, the fluid is diverted into low-permeability regions, similar to that observed in the 3D micromodel experiment. These results indicate that these nanohydrogels are also effective in modifying the conformance even in core samples. These particles clearly retain their stability for at least the 1 month period during the time that the swelling occurs. We did not test their stability over even longer time periods, which would be necessary for field applications, but we have no reason to expect that the particles degrade significantly over longer times.

3. CONCLUSIONS

In this work, we fabricate core−shell nanohydrogels with delayed swelling properties that can expand in volume under oil reservoir conditions. These swollen nanohydrogels behave as a yield stress fluid and divert water toward low-permeability zones of the porous medium. The hydrogel core-templated core−shell fabrication method features the formation of a degradable shell, which can protect core particles from immediate swelling in brine. This would greatly reduce any possible shear degradation at the well bore where the shear forces are the largest and would enhance particle transport through the rock near the well bore, thereby improving the utility of these nanohydrogels for conformance control deeper within the reservoir. Eventually, core particles can swell to more than 200 times their volume, taking over 30 days to do so. To demonstrate the capability of these nanohydrogels for fluid diversion, we inject the nanohydrogel brine suspension into a 3D glass-bead micromodel and visualize the flow profile using confocal microscopy. By comparing the flow pattern before and after nanohydrogel injection and swelling, we find the fluid flow is diverted into previously poorly swept regions. More importantly, the permeability of the micromodel is reduced by ∼30% after nanohydrogel swelling. To simulate the process of nanohydrogel injection into an oil reservoir, we perform a core flood test and confirm that the nanohydrogels

https://dx.doi.org/10.1021/acsami.0c09958
ACS Appl. Mater. Interfaces 2020, 12, 34217−34225

can be transported freely through a rock sample with low permeability while significantly decreasing its permeability upon swelling and possibly diverting the fluid inside the rock sample to low-permeability zones. These core−shell nanohydrogels that can swell in the reservoir have great potential as a conformance control agent in enhanced oil recovery applications. Further effort is required to ensure that they can be produced in sufficient quantity and a viable price point. This is particularly true given the current downturn in the price of oil; nevertheless, the historic cyclic nature of oil prices suggests that their utility may be much greater in the future. However, the basic concept of small-size particles that are easily transported deep within the reservoir and that then swell to become a viable conformance control material is established by this work.

4. EXPERIMENTAL SECTION

All chemicals are purchased from Sigma-Aldrich unless otherwise mentioned.

4.1. Fabrication of Core−Shell Nanohydrogels. Acrylamide (AM), acrylic acid (AA), 2-acrylamido-2-methyl-1-propanesulfonic acid sodium salt (AMPS, 50% in H_2O), (3-acrylamidopropyl)-trimethylammonium chloride (AMPTAC, 75% in H_2O solution), and *N*,*N*′-methylene bisacrylamide are dissolved in water with a concentration of 50 wt % and the pH of the solution is adjusted to 7 using NaOH. Ammonium persulfate (APS) as initiator is dissolved in water with a concentration of 0.05 wt %. This aqueous solution is emulsified with cyclohexane using a probe sonicator with a power of 40% to generate a water-in-oil emulsion. Span 80 (85548-250ML) is used as the surfactant to stabilize emulsions. We keep the solution at 65 °C for 1 h and then precipitate the particles into a large amount of ethanol and cyclohexane mixture with a volume ratio of 1:1 under vigorous stirring. To generate the shell, we add 1 ml of APS (0.5 wt %) aqueous solution into the mixture, and then add the shell monomers/crosslinker in the solution dropwise at a temperature up to 70 °C. The amount of the shell monomer depends on the shell thickness. The reaction is kept running for 20 h to complete the polymerization process. Afterward, we cool the mixture to room temperature, separate it by centrifugation, wash the particles several times, and dry the particles in a desiccator under vacuum for 48 h. For all of the core particles, the ratio of the four crosslinkers is at a fixed value. The molar ratio of acrylamide, acrylic acid, 2-acrylamido-2-methylpropane sulfonic acid, and (3-acrylamidopropyl)-trimethylammonium chloride is 34:5:4.75:4.

4.2. Nanohydrogel Core Size Control. The core size can be controlled by emulsification time for generating the emulsion, surfactant concentration for stabilizing the emulsion, and core monomer to crosslinker ratio. We keep the concentration of core monomers at 50 wt % to maintain high mechanical property and vary the total monomer to crosslinker molar ratio at 75:1, 160:1, and 300:1. We change the surfactant concentration from 1 to 5 wt % to stabilize the emulsion. For emulsification time, we use a high-power tip sonicator to generate the emulsion in an ice bath as the template and vary emulsification time from 3 to 5 min.

4.3. Nanohydrogel Shell Thickness Control. The shell thickness can be carefully controlled by varying the quality ratio between the shell monomer and the core particle. We take the radical polymerization efficiency on the core surface as 60%, and the density of the core and the shell is the same as it is a polymer-based core−shell particle. Therefore, the amount of the shell monomer plus the crosslinker can be calculated using the equation

$$M(\text{shell}) = \left(\left(\frac{R_2}{R_1}\right)^3 - 1\right) M(\text{core}) \tag{2}$$

where M(shell) is the mass of the shell, M(core) is the mass of the core, and R_2 and R_1 are the radius of the core−shell particle and the core, respectively. Then, the shell thickness is $\Delta R = R_2 - R_1$. Using this simple calculation, we load the amount of shell monomer with the crosslinker to the co-solvent while growing the shell and also extend the reaction time to make sure all of the shell monomers have been consumed. For each batch of samples, we maintain the reaction volume at 250 mL and weight at 1 g of core particle and increase the shell monomer quality to three times, six times, and nine times the total weight of core particle. For each experiment, we keep the solvent at a fixed volume of 250 mL, which can convert the amount of the shell materials into shell material concentration. For all samples, we use TEM to determine the diameters. A shell concentration with three times monomer quality (0.15 mol L^{-1}) can form a thin layer, which is ∼15 nm, while six times (0.5 mol L^{-1}) and nine times (0.9 mol L^{-1}) produce ∼25 and ∼40 nm shell, respectively. To synthesize a 30 nm shell, we increase shell monomer concentration up to 0.6 mol L^{-1}.

4.4. Rheological Measurement. We use an Ar-G2 rheometer to measure the rheological property of 1 wt % nanohydrogel brine suspension when nanohydrogels are just dispersed in brine and after immersing in brine for over a month at 50 °C until they reach the maximum swelling capacity. Before testing, the nanohydrogel is directly dispersed in brine with the assistance of a sonicator for 3 min. The geometry gap is 55 μm.

4.5. Fabrication of the 3D Micromodel. We prepare a rigid 3D micromodel porous medium by lightly sintering densely packed hydrophilic glass beads at 875 °C in thin-walled rectangular quartz capillaries. The 3D micromodel has a cross-sectional area A of 3 × 3 mm^2 and a length of the device of 3 cm. The average diameter of the beads is 150 μm with polydispersity 4% and porosity ∼41%. We also attach tubes to the inlet and outlet of the 3D micromodel and seal with 5 min epoxy. Before injecting the index-matching fluid, we put the whole device in a vacuum for 24 h and then slightly fill the device with CO_2. We fabricate another device following the same procedure with 63 μm glass beads with the same length and cross-sectional area as the 150 μm micromodel device.

4.6. Particle Tracking Velocimetry (PTV) in the 3D Micromodel. (1) An index-matching fluid (DMSO and water mixture with a volume ratio of 7:1) is injected into the 3D micromodel at a flow rate of 100 μL h^{-1}. The index-matching fluid contains a 543/633 nm fluorescent tracer particle with a size of 1 μm. We choose a *xy* position at the focal plane and record the tracer particle movement at 15 frames s^{-1} for 3 min. ImageJ is applied to stack all of the images into a single image as the flow pattern at this position. Other *xy* positions are also recorded following the same method. (2) The whole device is flushed with brine to remove all free tracer particles as much as possible. The composition of brine is 30 g L^{-1} NaCl, 7.5 g L^{-1} $CaCl_2$, and 5 mg L^{-1} $MgCl_2$. (3) Further, 1 wt %. nanohydrogels are dispersed in brine. We inject 1 pore volume of this brine suspension into the 3D micromodel. (4) The inlet and outlet of the 3D micromodel are sealed and the whole device is placed in an oven at 50 °C for 1 month, allowing them to reach the maximum capacity. Afterward, the brine is replaced after flushing with the index-matching solution for 10 h at 50 μL h^{-1}, and then step (1) is repeated, and the whole velocity map of the whole device is obtained using a confocal microscope.

4.7. Permeability of the 3D Micromodel before and after Nanohydrogel Swelling. We measure and calculate the permeability of the 3D micromodel by applying hydrostatic pressure, measuring the volumetric flow rate of the effluent fluid, and using Darcy's law.

4.8. Adsorption Study. We perform the adsorption test by flowing tracers (KBr, 1000 ppm) or nanohydrogels (10 000 ppm) into the core at day 1. The sample is collected at the end of the tube at a different time, and a spectrophotometer is used to analyze the concentration of nanohydrogels and tracers.

4.9. Process of "Core Flood" Test at the Shell Technology Center Houston. Core flood conditions: 6 in. (length) × 1 in. (diameter), Bentheimer core with permeability in brine of 1.2 Darcy at 50 °C and with a pore volume of 9.17 cm^3. The core is mounted in a Hassler style core holder at test conditions of 2000 psi (1.4 × 10^7 Pa), initial conditional pressure, and 1000 psi pre- or backpressure

https://dx.doi.org/10.1021/acsami.0c09958
ACS Appl. Mater. Interfaces 2020, 12, 34217−34225

(NCS of 1000 psi) at a temperature of 50 °C. (a) The nanohydrogel is dispersed in the brine, stirred at a low speed for 5 min, and then the nanohydrogel suspension is sonicated at room temperature for another 3 min to get a homogeneous particle suspension. (b) The particle suspension is injected into the core sample with a flow rate of 6×10^4 μL h^{-1}. (c) The whole "core" is sealed and incubated at 50 °C for over 40 days. Afterward, we reinject the brine in the device and record the pressure by a pressure transducer as a function of flow rate. For each flow rate, we obtain the mean pressure drop for each flow rate while calculating the permeability reduction.

4.10. Confocal Microscopy. We record the tracer particle motion in the 3D micromodel using a confocal microscope (Leica SP5). The excitation and/or emission for the tracer particle is 543/633 nm. Specifically, we use a 10× dry objective with a numerical aperture of 0.3 to acquire the fluorescent images. HeNe laser (543 nm) as the excitation source and the fluorescence signal is collected by photomultiplier tube (PMT) detectors through filters with 560/650 nm bandpass.

4.11. Scanning Electron Microscopy (SEM) and Transmission Electron Microscopy (TEM) Characterization. We use SEM (FESEM, Ultra55VP) and TEM (JEOL 2100) to characterize the morphology and structure of nanohydrogels. To prepare the samples, we disperse nanohydrogels in DI water with a low concentration. Afterward, a drop of the suspension containing nanohydrogels is deposited onto a silica wafer that sticks to the sample holder, and then the sample is freeze-dried using a lyophilizer (VirTis AdVantage Plus, SP Scientific) at a temperature of −80 °C and pressure 10^{-3} Pa for 5 h. After drying, we coat the samples with 5 nm thick platinum/palladium (Pt/Pd) using a sputter-coating machine (EMS 300T D Dual Head Sputter Coater). While imaging, the operation voltage is 5 kV. To prepare the TEM sample, we directly disperse the nanohydrogel suspension on the copper grid and let the sample dry.

■ ASSOCIATED CONTENT

Supporting Information

The Supporting Information is available free of charge at https://pubs.acs.org/doi/10.1021/acsami.0c09958.

Synthesis of 350 nm nanohydrogel with a 30 nm shell; viscosity of nanohydrogel suspension before swelling; adsorption study (PDF)

■ AUTHOR INFORMATION

Corresponding Authors

Lizhi Xiao − *State Key Laboratory of Petroleum Resources and Prospecting, China University of Petroleum, Beijing 102249, China*; Email: xiaolizhi@cup.edu.cn

David A. Weitz − *School of Engineering and Applied Sciences and Department of Physics, Harvard University, Cambridge, Massachusetts 02138, United States*; orcid.org/0000-0001-6678-5208; Email: weitz@seas.harvard.edu

Authors

Liyuan Zhang − *School of Engineering and Applied Sciences, Harvard University, Cambridge, Massachusetts 02138, United States*

Alireza Abbaspourrad − *Shell International Exploration and Production Inc., Shell Technology Center Houston, Houston, Texas 77082, United States*; orcid.org/0000-0001-5617-9220

Shima Parsa − *School of Engineering and Applied Sciences, Harvard University, Cambridge, Massachusetts 02138, United States*

Jizhou Tang − *School of Engineering and Applied Sciences, Harvard University, Cambridge, Massachusetts 02138, United States*

Flavia Cassiola − *Shell International Exploration and Production Inc., Shell Technology Center Houston, Houston, Texas 77082, United States*

Meng Zhang − *School of Engineering and Applied Sciences, Harvard University, Cambridge, Massachusetts 02138, United States*

Shouceng Tian − *State Key Laboratory of Petroleum Resources and Prospecting, China University of Petroleum, Beijing 102249, China*; orcid.org/0000-0002-9034-7504

Caili Dai − *School of Petroleum Engineering, State Key Laboratory of Heavy Oil Processing, China University of Petroleum (East China), Qingdao 266580, China*

Complete contact information is available at: https://pubs.acs.org/10.1021/acsami.0c09958

Author Contributions

L.Z., S.P., F.C., and M.Z. performed the experiments and, with D.A.W. designed the project. L.Z., A.A., and D.A.W. wrote the paper. J.T., S.T., C.D., and L.X. provided essential contributions and suggestions.

Notes

The authors declare no competing financial interest.

■ ACKNOWLEDGMENTS

This work was supported by the NSF (DMR-1708729), the Harvard MRSEC (DMR-1420570), China University of Petroleum, Beijing, and the Advanced Energy Consortium (www.beg.utexas.edu/aec/), whose member companies include ExxonMobil, Repsol, Shell, and Total. The authors also thank the Center for Nanoscale Systems at Harvard University for sample imaging.

■ REFERENCES

(1) Schulte, W. M. In *Challenges and Strategy for Increased Oil Recovery*, International Petroleum Technology Conference (IPTC 10146); IPTC, 2005; pp 1−9.

(2) Muggeridge, A.; Cockin, A.; Webb, K.; Frampton, H.; Collins, I.; Moulds, T.; Salino, P. Recovery rates, Enhanced oil Recovery and Technological Limits. *Philos. T. R. Soc. A* **2014**, *372*, No. 20120320.

(3) Zhang, C.; Oostrom, M.; Wietsma, T. W.; Grate, J. W.; Warner, M. G. Influence of Viscous and Capillary Forces on Immiscible Fluid Displacement: Pore-scale Experimental Study in a Water-wet Micromodel Demonstrating Viscous and Capillary Fingering. *Energy Fuels* **2011**, *25*, 3493−3505.

(4) Bai, B.; Liu, Y.; Coste, J.-P.; Li, L. Preformed Particle Gel for Conformance Control: Transport Mechanism Through Porous Media. *SPE Reservoir Eval. Eng.* **2007**, *10*, 176−184.

(5) Zhao, B.; MacMinn, C. W.; Juanes, R. Nonlocal Interface Dynamics and Pattern Formation in Gravity-Driven Unsaturated Flow Through Porous Media. *Proc. Natl. Acad. Sci. U.S.A.* **2016**, *113*, 10251−10256.

(6) Cueto-Felgueroso, L.; Juanes, R. Nonlocal Interface Dynamics and Pattern Formation in Gravity-driven Unsaturated Flow Through Porous Media. *Phys. Rev. Lett.* **2008**, *101*, No. 244504.

(7) Sheng, J. J.; Leonhardt, B.; Azri, N. Status of Polymer-flooding Technology. *J. Can. Pet. Technol.* **2015**, *54*, 116−126.

(8) Kamal, M. S.; Sultan, A. S.; Al-Mubaiyedh, U. A.; Hussein, I. A. Review on Polymer Flooding: Rheology, Adsorption, Stability, and Field Applications of Various Polymer Systems. *Polym. Rev.* **2015**, *55*, 491−530.

(9) Raffa, P.; Broekhuis, A. A.; Picchioni, F. Polymeric Surfactants for Enhanced Oil Recovery: A Review. *J. Pet. Sci. Eng.* **2016**, *145*, 723−733.

(10) Abdulbaki, M.; Huh, C.; Sepehrnoori, K.; Delshad, M.; Varavei, A. A Critical Review on Use of Polymer Microgels for Conformance Control Purposes. *J. Pet. Sci. Eng.* **2014**, *122*, 741−753.
(11) Hirasaki, G.; Miller, C. A.; Puerto, M. Recent Advances in Surfactant EOR. *Soc. Pet. Eng. J.* **2011**, *16*, 889−907.
(12) Yu, W.; Lashgari, H. R.; Wu, K.; Sepehrnoori, K. CO2 Injection for Enhanced Oil Recovery in Bakken Tight Oil Reservoirs. *Fuel.* **2015**, *159*, 354−363.
(13) Borling, D.; Chan, K.; Hughes, T.; Sydansk, R. Pushing Out the Oil With Conformance Control. *Oilfield Rev.* **1994**, *6*, 44−58.
(14) Zhou, Y. X.; Wu, X.; Sun, W.; Pu, S. H.; Zhao, J. X. Surfactant-Augmented Functional Silica Nanoparticle Based Nanofluid for Enhanced Oil Recovery at High Temperature and Salinity. *ACS Appl. Mater. Interfaces* **2019**, *11*, 45763−45775.
(15) Ranka, M.; Brown, P.; Hatton, T. A. Responsive Stabilization of Nanoparticles for Extreme Salinity and High-Temperature Reservoir Applications. *ACS Appl. Mater. Interfaces* **2015**, *7*, 19651−19658.
(16) Elsharafi, M. O.; Bai, B. Effect of Weak Preformed Particle Gel on Unswept Oil Zones/Areas during Conformance Control Treatments. *Ind. Eng. Chem. Res.* **2012**, *51*, 11547−11554.
(17) Wang, L. Z.; Geng, J. M.; Bai, B. J. Highly Deformable Nano-Cross-Linker-Bridged Nanocomposite Hydrogels for Water Management of Oil Recovery. *Energy Fuels* **2018**, *32*, 3068−3076.
(18) Ohms, D.; McLeod, J. D.; Graff, C. J.; Frampton, H.; Morgan, J. C.; Cheung, S. K.; Chang, K. T. Incremental-oil Success from Waterflood Sweep Improvement in Alaska. *SPE Prod. Oper.* **2010**, *25*, 247−254.
(19) Liu, Y. Z.; Bai, B. J.; Shuler, P. L. In *Application and Development of Chemical-Based Conformance Control Treatment in China Oil Fields*, SPE/DOE Symposium on Improved Oil Recovery, Tulsa (SPE-99641); SPE, Apr 22−26, 2006; pp 1−10.
(20) Pu, J. Y.; Zhou, J.; Chen, Y. S.; Bai, B. J. Development of Thermotransformable Controlled Hydrogel for Enhancing Oil Recovery. *Energ. Fuel.* **2017**, *31*, 13600−13609.
(21) Zaitoun, A.; Dupuis, G. In *Conformance Control Using SMG Microgels: Laboratory Evaluation and First Field Results*, In SPE Europec featured at 79th EAGE Conference and Exhibition (SPE-185864); SPE, June, 2017; pp 1−10.
(22) Zaitoun, A.; Tabary, R.; Rousseau, D.; Pichery, T. R.; Nouyoux, S.; Mallo, P.; Braun, O. In *Using Microgels to Shut Off Water in a Gas Storage Well*, SPE International Symposium on Oilfield Chemistry, Houston (SPE-106042); SPE, Feb 2−March 2, 2007; pp 1−8.
(23) Bai, B.; Li, L.; Liu, Y.; Wang, Z.; Liu, H. Preformed Particle Gel for Conformance Control: Factors Affecting Its Properties and Applications. *SPE Reservoir Eval. Eng.* **2007**, *10*, 415−422.
(24) Pritchett, J.; Frampton, H.; Brinkman, J.; Cheung, S.; Morgan, J.; Chang, K. T.; Williams, D.; Goodgame, J. In *Field Application of A New in-depth Waterflood Conformance Improvement Tool*, SPE International Improved Oil Recovery Conference in Asia Pacific, Kuala Lumpur (SPE-84897); SPE, Oct 20−21, 2003; pp 1−8.
(25) Jia, Y.; Yang, H.; Cheng, C.; Li, Z.; Hou, G.; Yuan, X.; Zhao, W.; Zhang, Z.; Liu, T. In *Field Application and Performance Evaluation of Polymer Microsphere Profile Control in Low Permeability Oil Reservoir*, SPE Abu Dhabi International Petroleum Exhibition & Conference, Abu Dhabi (SPE-197198); SPE, Nov 11−14, 2019; pp 1−12.
(26) Coste, J. P.; Liu, Y.; Bai, B.; Li, Y.; Shen, P.; Wang, Z.; Zhu, G. In *In-depth Fluid Diversion by Pre-gelled Particles, Laboratory Study and Pilot Testing*, Proceedings of the 2000 SPE/DOE Improved Oil Recovery Symposium, Tulsa (SPE-59362); SPE, Apr 3−5, 2000; pp 1−8.
(27) Yuan, C.; Varfolomeev, M. A.; Wei, J.; Zhao, S.; Cao, L. N. In *Deformable Micro-Gel for EOR in High-Temperature and Ultra-High-Salinity Reservoirs: How to Design the Particle Size of Micro-Gel to Achieve its Optimal Match with Pore Throat of Porous Media*, SPE Abu Dhabi International Petroleum Exhibition & Conference, Abu Dhabi (SPE-197804); SPE, Nov 11−14, 2019; pp 1−22.
(28) Dupuis, G.; Al-Maamari, R. S.; Al-Hashmi, A. A.; Al-Sharji, H. H.; Zaitoun, A. *Mechanical and Thermal Stability of Polyacrylamide-based Microgel Products for EOR*, SPE International Symposium on Oilfield Chemistry (SPE-164135); SPE, Apr 2013; pp 1−11.
(29) Partini, M.; Pantani, R. FTIR Analysis of Hydrolysis in Aliphatic Polyesters. *Polym. Degrad. Stab.* **2007**, *92*, 1491−1497.
(30) Baker, J. P.; Stephens, D. R.; Blanch, H. W.; Prausnitz, J. M. Swelling Equilibria for Acrylamide-based Polyampholyte Hydrogels. *Macromolecules* **1992**, *25*, 1955−1985.
(31) English, A. E.; Mafé, S.; Manzanares, J. A.; Yu, X.; Grosberg, A. Y.; Tanaka, T. Equilibrium Swelling Properties of Polyampholytic Hydrogels. *J. Chem. Phys.* **1996**, *104*, 8713−8720.
(32) Schweins, R.; K. Huber, K. Collapse of Sodium Polyacrylate Chains in Calcium Salt Solutions. *Eur. Phys. J. E: Soft Matter Biol. Phys.* **2001**, *5*, 117−126.
(33) Tong, D.; Yesiloz, G.; Ren, C. L.; Madhuranthakam, C. R. Controlled Synthesis of Poly(acrylamide-co-sodium acrylate) Copolymer Hydrogel Microparticles in a Droplet Microfluidic Device for Enhanced Properties. *Ind. Eng. Chem. Res.* **2017**, *56*, 14972−14979.
(34) Baker, J. P.; Hong, L. H.; Blanch, H. W.; Prausnitz, J. M. Effect of Initial Total Monomer Concentration on the Swelling Behavior of Cationic Acrylamide-based Hydrogels. *Macromolecules* **1994**, *27*, 1446−1454.
(35) Denisin, A. K.; Pruitt, B. L. Tuning the Range of Polyacrylamide Gel Stiffness for Mechanobiology Applications. *ACS Appl. Mater. Interfaces* **2016**, *8*, 21893−21902.
(36) Nyström, L.; A'lvarez-Asencio, R.; Frenning, G.; Saunders, B. R.; Rutland, M. W.; Malmsten, M. Electrostatic Swelling Transitions in Surface-bound Microgels. *ACS Appl. Mater. Interfaces* **2016**, *8*, 27129−27139.
(37) Zhu, D. Y.; Bai, B. J.; Jirui Hou, J. R. Polymer Gel Systems for Water Management in High-Temperature Petroleum Reservoirs: A Chemical Review. *Energy Fuels* **2017**, *31*, 13063−13087.
(38) Trappe, V. V.; Weitz, D. A. Scaling of The Viscoelasticity of Weakly Attractive Particles. *Phys. Rev. Lett.* **2000**, *85*, 449−452.
(39) Krummel, A. T.; Datta, S. S.; Münster, S.; Weitz, D. A. Visualizing Multiphase Flow and Trapped Fluid Configurations in a Model Three-dimensional Porous Medium. *AICHE J.* **2013**, *59*, 1022−1029.
(40) Datta, S. S.; Chiang, H.; Ramakrishnan, T.; Weitz, D. A. Spatial Fluctuations of Fluid Velocities in Flow Through a Three-dimensional Porous Medium. *Phys. Rev. Lett.* **2013**, *111*, No. 064501.

https://dx.doi.org/10.1021/acsami.0c09958
ACS Appl. Mater. Interfaces 2020, 12, 34217−34225